www.ietdl.org

Published in IET Generation, Transmission & Distribution
Received on 25th February 2013
Revised on 13th May 2013
Accepted on 20th June 2013
doi: 10.1049/iet-gtd.2013.0131

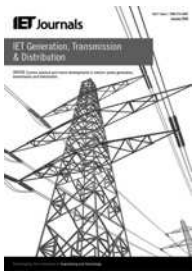

ISSN 1751-8687

Recognition of single and multiple partial discharge sources in transformers based on ultra-high frequency signals

Herman H. Sinaga[1], B.T. Phung[2], Trevor R. Blackburn[2]

[1]Department of Electrical Engineering, Lampung University, Bandar Lampung, Indonesia
[2]School of Electrical Engineering & Telecommunications, University of New South Wales, Sydney, Australia
E-mail: herman_sinaga@yahoo.com

Abstract: Partial discharge (PD) is a symptom of insulation defect or degradation in high-voltage equipment. Thus, PD detection is an important diagnostic tool. Furthermore in practical situations, the PD can be generated from a single or multiple sources. Being able to detect and classify such PD events will help to determine the necessary corrective action to prevent insulation breakdown. To demonstrate, three different simulated discharge conditions in transformers were investigated: void, floating metal and their combination. The PD signals were captured using an ultra-high frequency (UHF) sensor and denoised using wavelet transform method by application of Matlab wavelet multi-variate denoising tool. Two types of mother wavelet, that is, db and sym, were applied to decompose the signals and extract the signal features in terms of their skewness, kurtosis and energy. These features were then used as input to train a neural network to analyse and determine the PD source type. Results show this technique is able to classify and recognise single and multiple PD source types with a high degree of success.

1 Introduction

In power transformers, partial discharge (PD) is a symptom of insulation defect or degradation, which if left untreated over time will cause a catastrophic failure. To prevent transformer failure and ensure reliable performance, it is important to be able to determine accurately the condition of the transformer through monitoring its PD activities.

Ultra-high frequency (UHF) sensors can be used to detect the PD signals. The UHF detection method has a number of advantages over other detection methods such as the conventional electrical detection method in the lower range of the frequency spectrum (up to ~1 MHz) as defined in the IEC-60270 Standard [1–3]. It is possible to achieve better sensitivity by using the UHF detection method [4]. Also, it gives better immunity against interference from air corona which is a common problem associated with on-site monitoring [5].

PDs can arise from a single or multiple defects within the insulation structure. Since different types of defects usually produce different PD waveforms [1], it is possible to recognise the sources of the PD from its measured signal. Various analysis techniques based on the UHF signals have been investigated to recognise the PD sources. A wavelet analysis method was proposed by [6, 7] to recognise multiple PDs in power transformers. However, this method requires substantial computation which slows down the recognition process. To alleviate this problem, [8, 9] proposed the use of envelope analysis to distinguish between partial discharges. It was asserted that the envelope of the PD signals can be utilised as a PD signature and hence a similarity function is applied to distinguish the PD sources. In another investigation [10], a method was proposed to classify the PD events in GIS by extracting the PD features from the UHF signals. Here, the signals were decomposed by using wavelet transforms, and then the PD features were extracted from the decomposed signal. This method gives a fast and accurate classification of the GIS PD events, and also it was able to separate air corona from the PD signals. Further work was carried out using wavelet-based denoising to combat the presence of embedded noise in the measured signals [11]. In addition to removing the noise, the threshold value method was also applied. This was intended to remove the white noise that was not able to be eliminated by the previous denoising step [11]. Although this denoising method is able to remove the suspected white noise, the process can also alter the PD signals. This resulted in further investigations for other PD signal denoising methods [12–14]; all these are based on univariate analysis.

In this paper, the multivariate approach to denoise multiple signals by utilising the relationship between signals is applied for recognition of single and multiple PD sources in transformer insulation. The PD signals were recorded by using a UHF sensor to capture the electromagnetic waves emitted by the PD source. The obtained UHF signals were denoised by applying the wavelet multivariate denoising method [15]. After the signals are denoised, they are decomposed into five levels by using wavelet. Then three features, namely kurtosis, skewness and energy, are extracted from the decomposed signal. The J criterion [10]

is applied to determine the best features node composition. Two types of mother wavelet are used for denoising and decomposing the PD signals, that is, db and sym. The extracted features are then used as inputs into a neural network to classify and recognise the PD sources.

2 UHF sensor

Electromagnetic waves are emitted from PD sources because of very short current pulses generated during the discharge process. They span a wide frequency spectrum including a range from a few hundred MHz to a few thousand MHz, otherwise known as the UHF band. Using appropriately-designed UHF sensors (antennas), the electromagnetic signals can be detected and recorded by a measuring device connected to the sensor. As the signals have to propagate through various physical media inside the transformer tank, they are refracted and reflected by complex interior obstacles such as windings, the core structure and the transformer tank itself.

For power transformer monitoring, the UHF sensor is inserted into the transformer tank to capture the electromagnetic waves emitted by the PD source. There are two ways of installing the sensor: via the oil drain valve [16] or the dielectric window [17]. The size of the oil drain valve imposes a constraint on the sensor dimension, whereas the dielectric window can be created with an appropriate size to accommodate the sensor. However, the placement of a dielectric window sensor needs an additional hole to be made on the transformer tank. As for the oil valve sensor, this is not required because the sensor can be easily retrofitted into the transformer via the existing built-in oil drain valve [16].

For inserting via the oil drain valve, the size of the sensor is limited by the diameter and length of the oil drain. The shape of the sensor can be a short monopole [8, 16], plate, zigzag or conical [16, 18] as long as it is able to be fitted through the drain valve. The sensitivity of this kind of sensor is affected by the depth of the sensor insertion [16]. The deeper the sensor is inserted, the higher the magnitude of the PD signals acquired. However, the sensor must not initiate breakdown because of the high electric stress at the tip of the sensor [17].

For a dielectric window, the sensors usually have a planar shape [17]. The sensor can be a micro-strip sensor [19, 20], log-spiral or spiral [17, 21]. This kind of sensor is usually etched on the surface of a dielectric material, using the same process as in making electronic printed circuit boards (PCB). The sensor is etched on the PCB with dimensions proportional to the working frequency of the sensor.

The planar shape sensors tend to have better frequency response characteristic than the monopole [22], thus in this paper a planar shape type which is a log-spiral sensor with dual-arms was chosen and used in the experiment. The sensor is a tapered log-spiral shape etched onto the surface of a single layer PCB and a six-section balun is used for bridging the sensor to the 50 Ω coaxial cable. The number of turn of the log-spiral arm is 1.5 with a 10 cm diameter.

2.1 Log-spiral sensor

The log-spiral sensor arm is calculated using the pair equations below

$$r_1 = r_0 e^{a\phi} \tag{1}$$

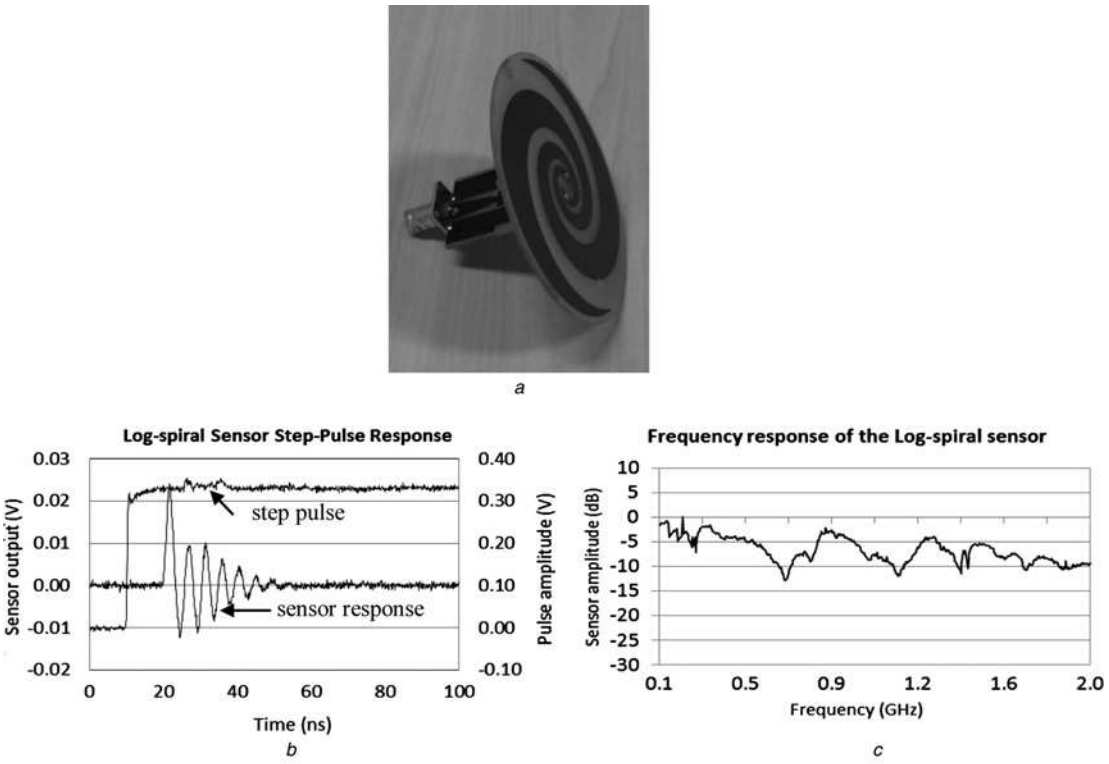

Fig. 1 *Fabricated sensor and its response to the step pulse and the frequency response of the sensor*

a Dual arms log-spiral sensor
b Sensor response to a step pulse
c Frequency response

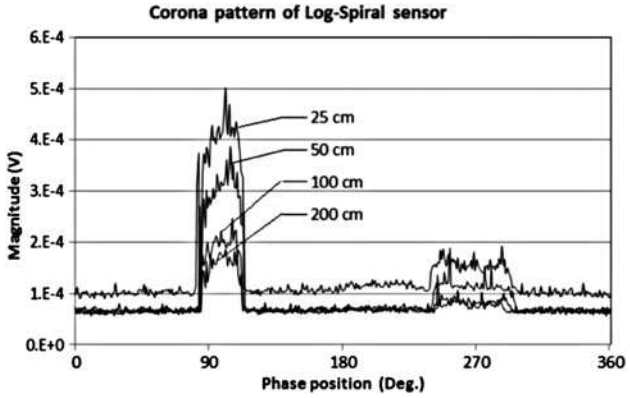

Fig. 2 *Phase-resolved patterns recorded using Log-spiral sensor at varying distance from the source*

$$r_2 = r_0 e^{a(\phi-\phi_0)} \quad (2)$$

where r_1 denotes outer radius of the spiral, r_2 is inner radius of the spiral, r_0 is initial outer radius of spiral, a is the rate of spiral growth and ϕ denotes the angular position. The number of arms is set to 2, and for this reason it is called dual-arms log-spiral sensor. The number of turns is 1.5 which produces an adequate radiation pattern [23]. The end of the spiral arms is designed with tapered end. The size of the sensor is 10 cm in diameter and it is constructed using commercially available FR4 substrate (Fig. 1*a*).

2.2 Sensor pulse response

The sensor step pulse and frequency responses were evaluated using a custom-made TEM cell. This cell was designed to match the sensor impedance (i.e. 50 Ω) and simulate the propagation mode of PD in the transformer. The input pulse has rise-time of 0.5 ns and was maintained for a long duration so the sensor response was only because of the changed input voltage. Figs. 1*a* and *b* show the fabricated sensor and its response to the step pulse. The frequency response of the sensor, measured from 100 MHz up to 2 GHz, is shown in Fig. 1*c*. Over this frequency range, the response is reasonably stable and attenuation is mostly within 10 dB.

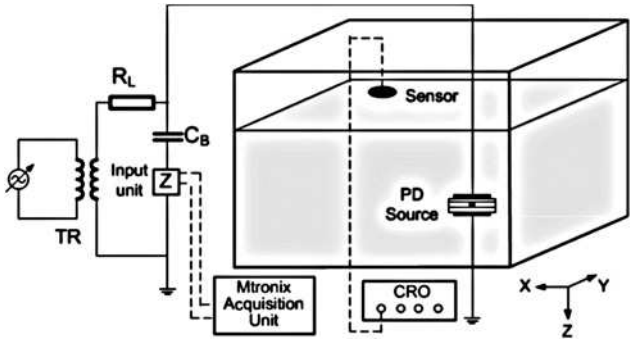

Fig. 3 *Experiment diagram of PD signals detection and recording*

2.3 Sensor sensitivity to detect corona signals

To check the sensor ability to pick up electromagnetic signals, corona produced by a needle to ground plane electrode arrangement is chosen as the PD source. The resultant discharges are very stable in magnitude. However, their major frequency components are below 200 MHz, that is, below the UHF range. Nevertheless, the sensor was still able to detect the corona signals and all tested sensors showed this ability.

Fig. 2 shows the phase-resolved patterns with the sensor installed at varying distance from the corona source.

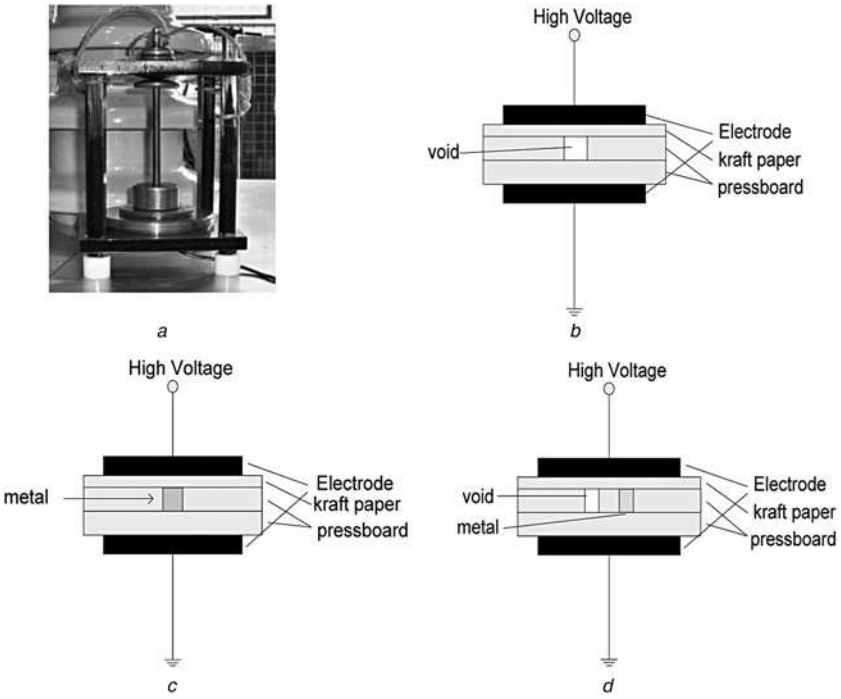

Fig. 4 *PD models*

a Electrodes and defects
b Void
c Floating metal
d Mixture of void and floating metal

doi: 10.1049/iet-gtd.2013.0131

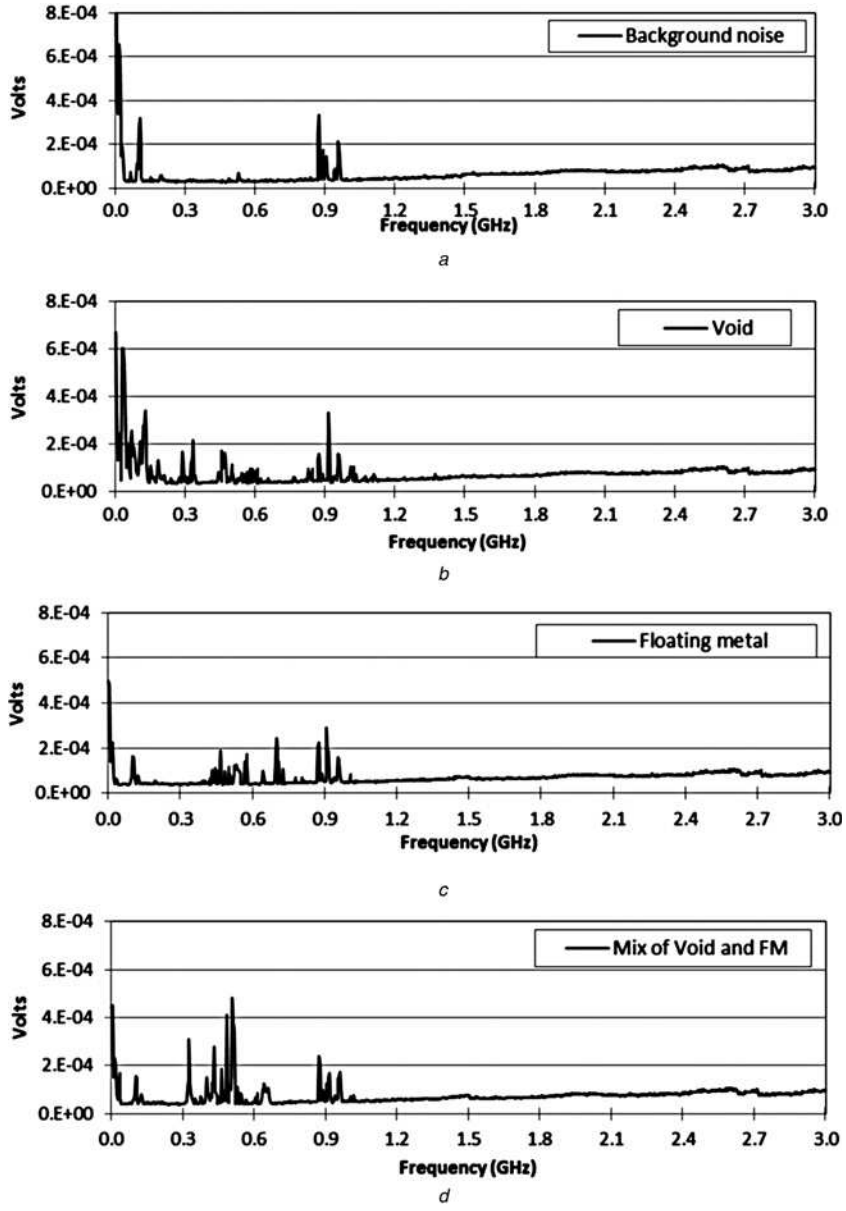

Fig. 5 *Full span spectra of*

a Background noise
b Void defect PD
c Floating metal PD
d PD signals produced by combination of void and floating metal

Discharges as low as 5 pC and at a distance up to 2 m can be detected. This is well within the acceptance criterion of the PD test for power transformers, that is, 500 pC according to IEC 60076.3 Standard. Thus the sensor can provide a viable means for detecting PDs in practical applications.

3 UHF PD signals

The UHF PD technique detects and measures the electromagnetic pulses emitted by the PD sources. These pulses have a very short duration, typically < 1 ns of rise time and a few ns of pulse width. Thus in terms of frequency, it is a broad band signal which contains components well into the GHz range, that is, covering the UHF frequency band (300 MHz–3 GHz). In this paper, a log-spiral UHF sensor was constructed and used to capture the PD signals. The sensor captures those frequency components of the signal that fall within its working frequency range. In addition, it will pick up other unwanted noise/interference present in the same frequency band. This will adversely affect the analysis result. Therefore it is important to improve the signal-to-noise ratio (SNR) by removing the noise as much as possible before doing further analysis. The SNR in dB is given by

$$\mathrm{SNR} = 10 \log\left(\frac{P_{\mathrm{signal}}}{P_{\mathrm{noise}}}\right) \tag{3}$$

where P_{signal} denotes the average power of the PD signal and P_{noise} is the average power of the noise. Owing to the inherently stochastic behaviour of PDs, their signals will have varying amplitudes. Furthermore, the PD level also varies with different PD defect types. Consequently for a given level of ambient noise background, the SNR will

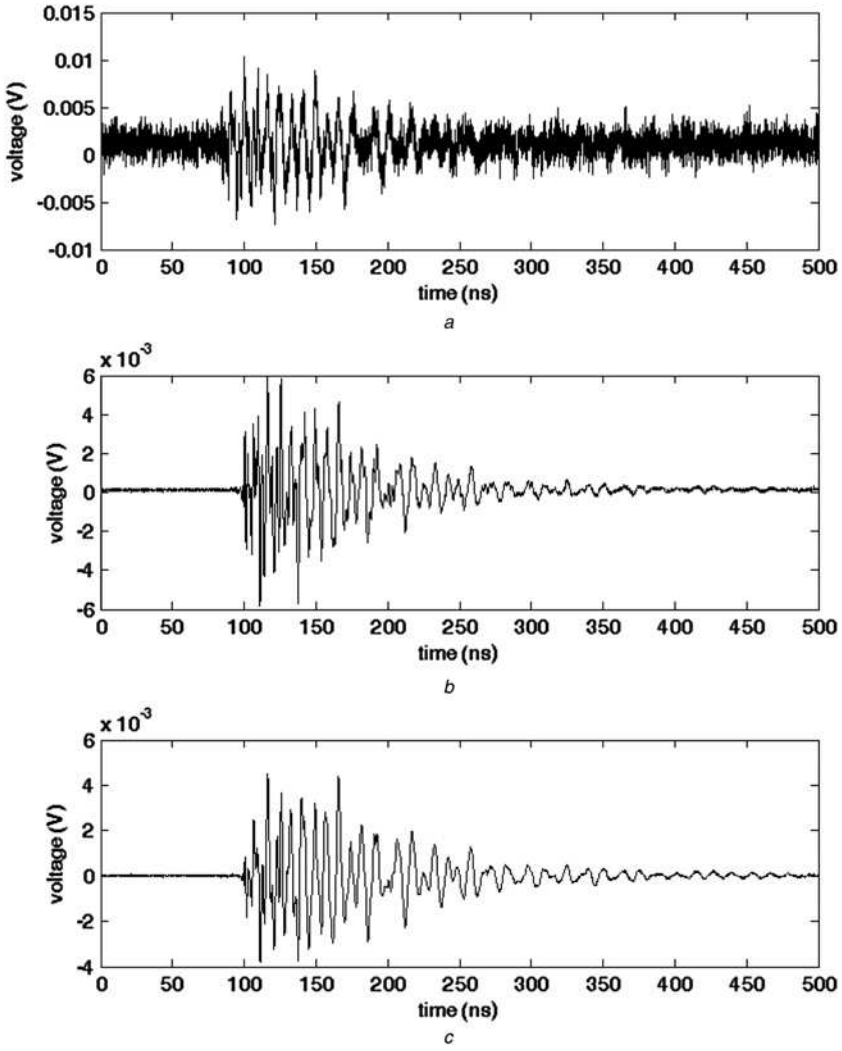

Fig. 6 *Typical example of the denoising process*

a Original signal
b Denoised using multivariate thresholding
c Result after retaining PCA component

vary. In this paper, the SNR value of the PD signals obtained from the laboratory experiment extends from as low as 0.44 dB to as high as 29.30 dB.

3.1 UHF PD detection

Three PD defect models were constructed to simulate discharges because of a void, floating metal (FM) and a combination of both. The PD defect models were built using three layers of solid insulation material sandwiched between two flat electrodes: two layers of pressboard and a layer of Kraft paper on top. The middle layer of pressboard was punctured to create a hole with diameter of 0.5 mm. For floating metal sample, a metal plate was fitted into the hole. Figs. 3 and 4 show the experiment diagram and the PD defect models. All samples were immersed in oil inside a fully covered distribution transformer tank in the laboratory.

A log spiral sensor (antenna) was fitted through a small opening at the top of the transformer tank to capture the electromagnetic signal emitted by the PD defect models. The sensor output was connected to an oscilloscope to digitise the signal, and the captured data were transferred to a computer for processing and analysis. The sensor output was also connected in parallel to a spectrum analyser for recording the frequency spectra of the electromagnetic signals. In order to capture the fast and wide frequency range of the partial discharge, an oscilloscope with bandwidth of 4 GHz and sampling rate up to 40 GS/s was used. A spectrum analyser with frequency range from 9 kHz up to 3 GHz was also used to record the PD signals in frequency domain.

The applied test voltage was set to 6.5 kV for void, 7 kV for floating metal and 8 kV for a combination of void and floating metal. A higher voltage was set for the mixed model to ensure PD will occur in both defects. Also shown in Fig. 3 is a conventional PD system (Mtronix), used as the benchmark for verifying the occurrence of PDs and their measurements. To confirm no discharges occurred from other sources such as surface discharges from the test sample itself, a 'plain' sample without void or floating metal was used for checking. It was verified that the inception for surface discharges was more than 11 kV, well above the voltage levels used in testing the defect models.

3.2 PD signal spectrum

The frequency range of emitted PD signals is influenced by the physical nature of the PD source [24] and the applied

doi: 10.1049/iet-gtd.2013.0131

voltage level [25]. Fig. 5 shows the typical spectra of PD signals for each type of defect models. These were recorded by operating the spectrum analyser under full span mode to capture the signals spectra over the maximum frequency range. The presence of the PD signals can be discovered by comparing the background noise spectrum (Fig. 5*a*) against that with the defect present [26].

The experiment was conducted using an enclosed transformer tank. However, some external noise can still enter the tank and be picked up by the sensor. The background spectrum (i.e. without any PD source) shows that there are two distinct groups of interference that can be easily spotted, that is, at around 900 MHz and under 100 MHz. Other signals associated with communication broadcast also can be noted at around 400–500 MHz, although not as high as the two groups mentioned earlier.

Fig. 5*a* shows the spectrum of background noise, captured using a spectrum analyser set to full-span recording mode. Figs. 5*b–d* show the typical spectra of various PD defect models used in the experiment which also include the background noise. The spectra of the PD signals can be extracted by subtracting the noise components. It can be seen that the void defect emits EM signals mainly below 500 MHz while the floating metal can generate frequency components up to 750 MHz. Note that for the combination of void and floating metal, the applied voltage was set higher to ensure discharges in both defects. This results in higher discharges as evident in the magnitude of the observed spectrum in Fig. 5*d*.

3.3 Multivariate denoising

The UHF detection method is targeted to capture the fast electromagnetic transient signals emitted by PD events. However, the pick-up signals are very small even for a well-designed UHF sensor. This situation is further exacerbated by the interference from unwanted signals or noise. Typical interferences in the UHF range consist of digital radio, television and telecommunication signals, thermal noise in the detection system and periodic pulses from switching operations [12–14]. In order to improve the detection sensitivity, it is necessary to denoise the PD signals to remove the unwanted signals. In this paper, this is done by using multivariate denoising tool.

Multivariate wavelet denoising deals with the regression models of the form

$$X(t) = f(t) + \varepsilon(t),\ t = 1, ..., n \tag{4}$$

where $(X(t))_{1 \le t \le n}$ denotes the observed signals, $\varepsilon(t)_{1 \le t \le n}$ represents the centred Gaussian white noise of unknown variance σ^2 and $f(t)$ denotes the unknown function to be recovered.

The multivariate denosing method is a useful tool to denoise multiple signals as it exploits the relationships between the signals to provide additional denoising effect [15]. The multivariate denoising procedure can be carried out in four steps as follows:

1. Perform wavelet transform at level J for all columns of X. This step produces matrices $\boldsymbol{D}_1,\ldots,\boldsymbol{D}_J$ which contain detail of coefficient at level 1 to J of the p signals, and approximation coefficients $\boldsymbol{A}_j$ of the p signals.
2. Remove noise by a simple multivariate thresholding after a change of basis. The noise covariance estimator is calculated using minimum covariance determinant of the matrices $\boldsymbol{D}_J$ and defined as $\hat{\Sigma}_\varepsilon = \mathrm{MCD}(\boldsymbol{D}_1)$ and is used to compute matrix $\boldsymbol{V}$ such that $\hat{\Sigma}_\varepsilon = \boldsymbol{V}\Lambda\boldsymbol{V}^{\mathrm{T}}$ where $\Lambda = \mathrm{diag}(\lambda_i,\ 1 \le i \le p)$. Apply to each detail after change of basis, the p univariate thresholding using threshold $_{\mathrm{q}}$ for each ith column. Fig. 6*a* shows a typical example of a raw signal with a SNR of 1.03 dB and Fig. 6*b* is the output of this step. The denoised signal using a simple multivariate thresholding shows a satisfactory result. However, it can still be further improved.
3. Improve the obtained result by applying principal component analysis (PCA) and retaining fewer principal components. Perform PCA of the matrix $\boldsymbol{A}_J$ and select the appropriate number p_{J+1} of useful principal components.
4. Reconstruct the denoised matrix $\check{\boldsymbol{X}}$ from the simplified detail by inverting the wavelet transform. Fig. 6*c* shows a typical result of this step.

4 Signal features extraction and recognition

Fig. 7 shows the flowchart diagram for the signal processing and recognition of PD sources. The process is divided into five stages: signal denoising, signal decomposition, feature extraction, features evaluation/selection to choose the most separable features, and classification. Signal denoising is done by applying the multivariate denoising method. Each group of PD data was denoised by using Matlab wavelet multivariate denoising software tool. The processed data were then decomposed to five levels, and thus producing a total of 63 nodes. Fig. 8 shows a typical decomposition of a floating metal denoised signal and its data for node (2, 1), (5, 0) and (5, 26) together with the denoised signal. For both processes of denoising and decomposing, two different mother wavelets were used, that is, db and sym. The mother wavelet of order 2 was chosen based on its effectiveness in removing noise encountered in this work [15]. Choosing a higher order will consume substantially more computing time.

Feature extraction is applied to reduce the number of inputs for the neural network training. In this paper, three features were extracted from each node: skewness, kurtosis and

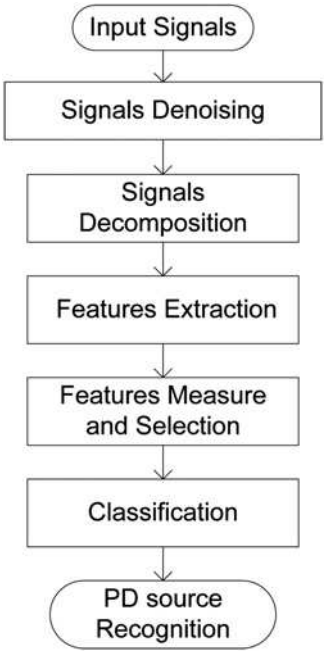

Fig. 7 *Flowchart of the data processing*

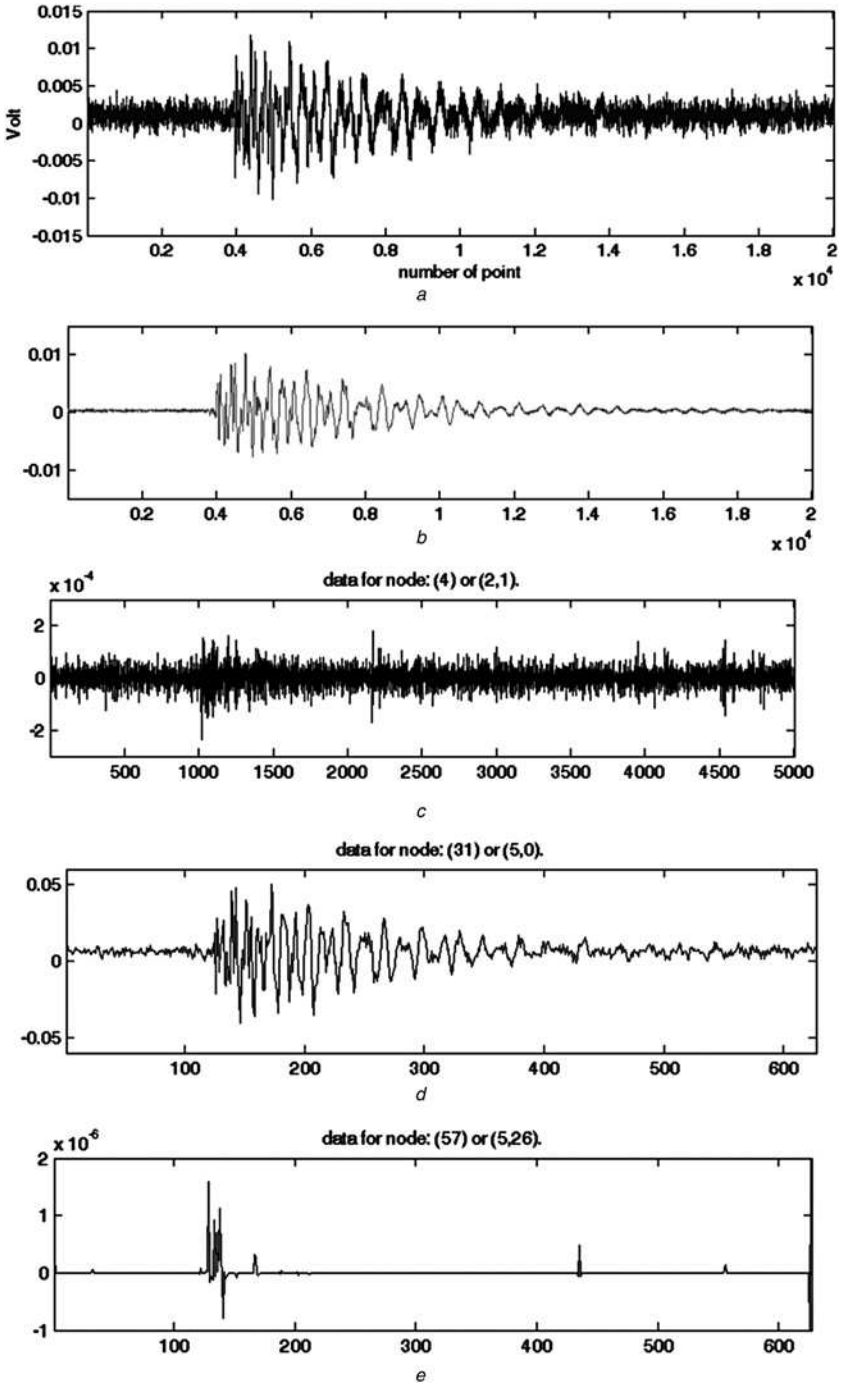

Fig. 8 *Signal decomposition*

a Original FM signal
b Denoised signal
c Node (2,1)
d Node (5,0)
e Node (5,26)

energy. Skewness is a parameter expressing the asymmetry of the data around the sample mean. Kurtosis shows how sharp the distribution of the data is. Energy indicates the percentage of the signal energy of each node.

The skewness and kurtosis are formulated as follows [10]

$$S_{j,n} = \frac{\sum_k (\varpi_{j,k,n} - \mu_{j,n})^3}{(N_{j,n} - 1)\sigma_{j,n}^3} \tag{5}$$

$$K_{j,n} = \frac{\sum_k (\varpi_{j,k,n} - \mu_{j,n})^4}{(N_{j,n} - 1)\sigma_{j,n}^4} - 3 \tag{6}$$

where $\varpi_{j,k,n}$ is the kth coefficient of node (j, n), $\mu_{j,n}$ is the mean deviation value, $N_{j,n}$ is the length of the coefficient array $\varpi_{j,n}$ and $\sigma_{j,n}$ is the standard deviation value.

The energy value of each node is calculated as

doi: 10.1049/iet-gtd.2013.0131

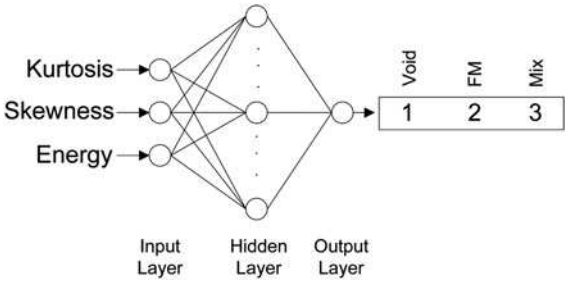

Fig. 9 *Three-layer neural network*

$$e_{j,n} = \left|\varpi_{j,n}\right|^2 \tag{7}$$

where $\varpi_{j,n}$ is the wavelet packet coefficient of node (j, n)

The total number of signals acquired from the experiment is 600, that is, 200 data records for each PD defect type and from which 150 data were used as the training input and 50 for testing of the neural network scheme. Altogether, 450 data were used for training and 150 data were used for testing. From each node three features were extracted, and thus produced a total of $3 \times 63 \times 450 = 85\,050$ training data. This is a fairly large amount of data for use as neural network training input. Besides, the inclusion of undesirable data features can make the classification process more difficult. Therefore the number of data must be reduced by using only the features that preserve maximum separability.

To determine the node with the feature that has the most separable value, a criterion known as J criterion is used [10]. J criterion compares the extent of scattering of feature values for between-class and within-class. The best node with the largest J value is selected as the input for the neural network. The criterion is defined as

$$J(j,\ n) = \frac{S_b(j,\ n)}{S_w(j,\ n)} = \frac{\sum_{c=1}^{L} \frac{N_c}{N}(m_c(j,\ n) - m(j,\ n))^2}{\sum_{c=1}^{L} \frac{N_c}{N}\sigma_c^2(j,\ n)} \tag{8}$$

where S_b denotes between-class scatter value, S_w is within-class scatter value, N_c is number of samples belong to class c, N is number of total samples, $m_c(j, n)$ is mean values of feature at node (j, n) for class c, $m(j, n)$ is mean values of feature at node (j, n) for all samples and σ_c (j, n) is variance of the features at node (j, n).

After the best node was selected, the features from its node were input into a feed-forward neural network to train the back-propagation learning rule for PD recognition. Fig. 9 shows the structure of the multi-level perceptron neural network.

The feed-forward neural network used has three inputs. The output as shown in the figure has 1 layer – a linear type which is associated with void as 1, floating metal as 2 and mix of void and FM as 3.

5 Result and discussion

A total of 600 UHF signals were recorded in the experiment for the three PD types. Thus, there are 200 records for each PD source. The measured signals were denoised by applying the multivariate denoising method through a Matlab function. A typical denoising result is shown in Fig. 10. It can be seen that the irregular spikes have been removed. This is particularly evident over the time period prior to the arrival of the PD signals. However, it was noted that there is a slight reduction in the PD magnitude.

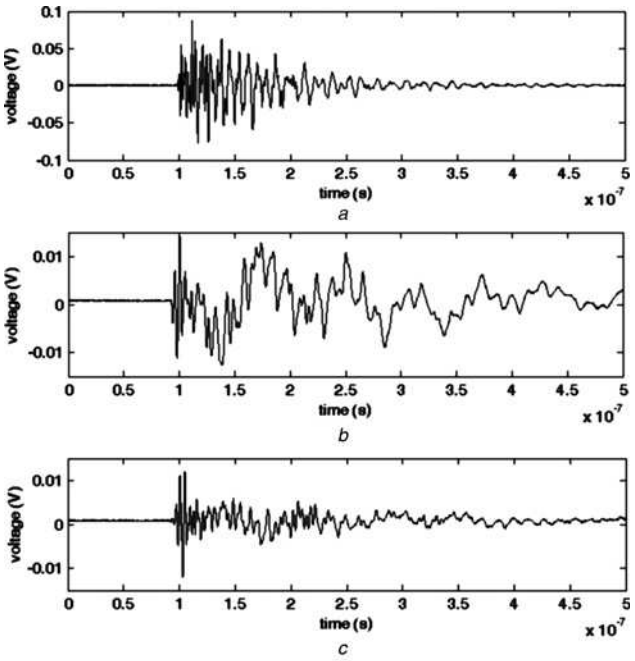

Fig. 10 *Denoised PD signals using db2 wavelets*

a FM
b Void
c Mix of FM and void

The denoised signals are then decomposed to five levels and produced 63 nodes. From each node three features were extracted, that is, kurtosis, skewness and energy. The J criterion is used to determine the node that will be used as the neural network input. The same mother wavelet was used to denoise and decompose the signals. Both db2 and sym2 wavelets resulted in the same total J values and nodes. These are summarised in Table 1.

Fig. 11 shows the features plot of the best nodes using db2 and sym2 wavelets. Both wavelets resulted in the same best nodes, determined by applying the J criterion formula. It can also be seen that by using the J criterion, the features can be clustered together for each PD source. For floating metal and void, all the feature values are totally separated. As for the combination of both defects, some feature values are very close to those associated with the single defects.

A feed-forward neural network with back propagation was used to classify the source of the PDs. The network had two hidden layers, where each hidden layer has 20 neurons of sigmoid type, and the training error was set to 0.01. The data set (600 in total) was divided into two groups: 450 data for use as training input to train the neural network, and 150 data as testing input using the trained network to classify the PD sources. Classification was done for both

Table 1 Largest J values of the three features

Feature	Node, db2	Node, sym2	J max, db2	J max, sym2
kurtosis	(5,0)	(5,0)	2.7611	2.7611
skewness	(2,1)	(2,1)	3.0516	3.0516
energy	(5,26)	(5,26)	2.0104	2.0104

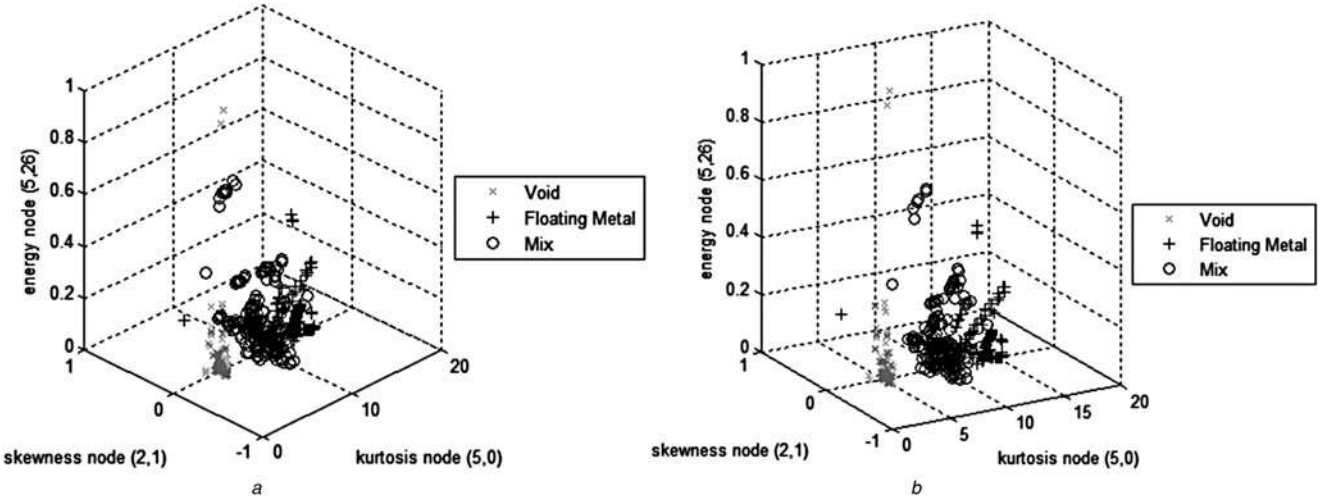

Fig. 11 *Features plot of the best nodes using different wavelets, denoised using*
a db2
b sym2

features that were obtained using db2 and sym2 wavelets as shown in Fig. 7. The results, summarised in Table 2, show that the single and multiple PD sources can be classified and thus recognised with high success rate.

5.1 PD signals denoising effect

The denoising process is one of the most time-consuming steps in this recognition process. In addition, denoising might remove some useful parts of the PD signals and cause incorrect recognition. Thus it is important to verify that the denoising process was of benefit to the recognition results.

By using a similar recognition process as shown in the flowchart in Fig. 6, except that the denoising process was excluded, the results now show different nodes as the best ones: nodes (5, 0), (2, 1) and (5, 16) for kurtosis, skewness and energy, respectively. The same best nodes were produced by both mother wavelet types. The features plot of the best nodes after decomposition is shown in Fig. 12.

Table 2 Percentage of correct classification using feed-forward neural network

PD type	Number of sample	Correct classification		
		Denoised		Un-denoised
		db2	sym2	
void	50	50	50	50
FM	50	45	45	22
mix of void & FM	50	48	48	41
correctness (%)		95.3	95.3	75.3

It shows poorer separation as compared with the 'original one', evident by the overlapping value of each feature of the mixed and the floating metal. This poor separation causes the recognition result of the un-denoised case to be lower whereas for the denoised one, the result as shown in Table 2 shows significant increase of the correct recognition

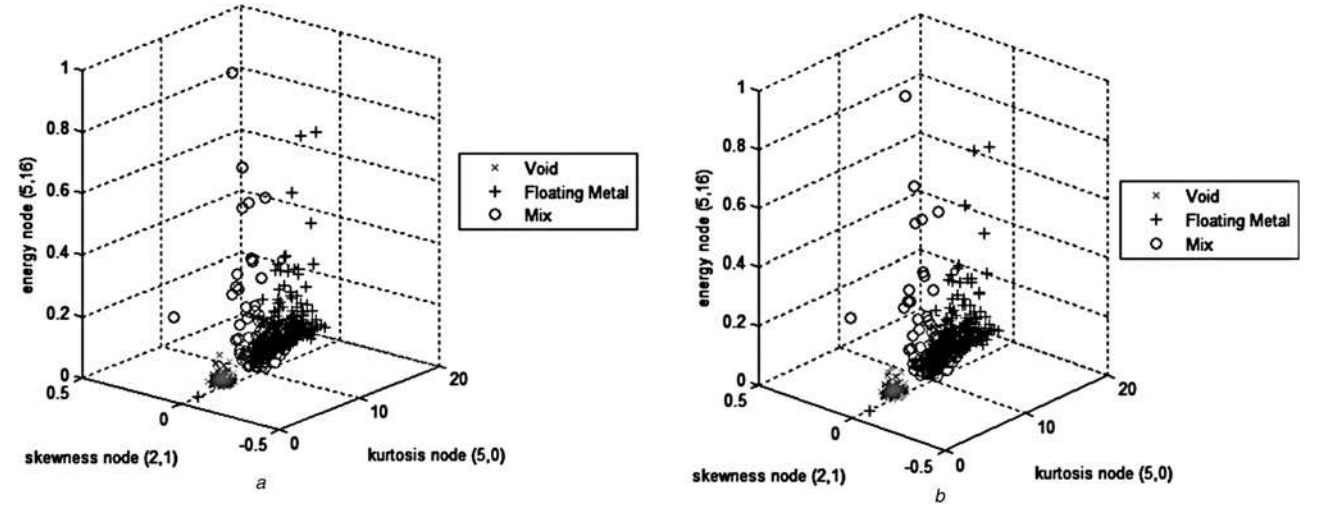

Fig. 12 *Features plot of best nodes without denoising using different wavelets*
a db2
b sym2

doi: 10.1049/iet-gtd.2013.0131

for both types of mother wavelet. The mix of void and FM type shows the most significant improvement, from 22 correct (undenoised) to 45 correct (denoised). The overall percentage correctness without the denoising process is 75.3% but it increases to 95.3% after applying the multivariate denoising tool.

It should be stressed that this work was developed in the laboratory environment. For proof-of-concept, further field testing is needed in order to prove the proposed algorithm is viable for practical applications. In terms of hardware requirement, the components to build the system are readily available. UHF sensors for PD measurement in transformers are already available commercially. It is expected such sensors can also be used in this particular application for PD defect recognition. The PD waveforms can be accurately captured using either high-end digital oscilloscopes or digitiser unit with built-in computer (bandwidth of 4 GHz and sampling rate of 40 Gs/s).

6 Conclusions

PD sources caused by different types of single or multiple defects generate different signal patterns. This paper discussed the recognition of single and multiple PD sources in transformer insulation. The PD signals were captured using an UHF sensor and recorded using both a spectrum analyser and an oscilloscope. The presence of noise/interference will adversely affect the analysis result. Thus it is important to denoise the recorded signals before further analysis can be carried out. As compared with other published techniques, the approach in this paper is different in that wavelet multivariate denoising is utilised to clean up the PD signals before the features are extracted for classification. This will improve the correct classification rate of the PD source.

Three features were extracted from the PD signals, and used as inputs into a neural network to recognise the PD sources. The features were extracted from the decomposed signal components. The J criterion was applied to determine the best nodes, that is, those that give the most separability of the features. For both the de-noising and decomposing steps, similar wavelets were applied (db2 and sym2) and resulted in similar J values and nodes.

Using a feed-forward neural network, it was demonstrated that single and multiple PD events can be classified and thus recognised by the proposed method. It was also shown that the overall percentage correctness is significantly improved with the application of signal denoising prior to classification.

7 References

1 Bartnikas, R.: 'Partial discharges – their mechanism, detection, and measurement', *IEEE Trans. Dielectr. Electr. Insul.*, 2002, **9**, (5), pp. 763–808

2 Stone, G.C.: 'Partial discharge diagnostics and electrical equipment insulation condition assessment', *IEEE Trans. Trans. Dielectr. Electr. Insul.*, 2005, **12**, (5), pp. 891–904

3 Judd, M.D., Yang, L., Hunter, I.B.B.: 'Partial discharge monitoring for power transformers using UHF sensors part 1: sensors and signal interpretation', *IEEE Electr. Insul. Mag.*, 2005, **21**, (2), pp. 5–14

4 Raja, K., Floribert, T.: 'Comparative investigations on UHF and acoustic PD detection sensitivity in transformers'. Proc. ISEI, Boston, MA, USA, April 2002, pp. 150–153

5 Judd, M.D., Yang, L., Hunter, I.B.B.: 'Partial discharge monitoring for power transformers using UHF sensors part 2: field experience', *IEEE Electr. Insul. Mag.*, 2005, **21**, (3), pp. 5–13

6 Yang, L., Judd, M.D.: 'Recognising multiple partial discharge sources in power transformers by wavelet analysis of UHF signals', *IEE Proc. Sci. Meas. Technol.*, 2003, **150**, (3), pp. 119–127

7 Lupò, G., Petrarca, C., Vitelli, M., Angrisani, L., Daponte, M.: 'Analysis of ultrawide-band detected partial discharges by means of a multiresolution digital signal-processing Method', *Meas. – J. Int. Meas. Confederation*, 2000, **27**, (3), pp. 207–221

8 Pinpart, T., Judd, M.D.: 'Differentiating between partial discharge sources using envelope comparison of ultra-high-frequency signals', *IET Sci. Meas. Technol.*, 2010, **4**, (5), pp. 256–267

9 Pinpart, T., Fletcher, J.E., Judd, M.D.: 'Methods for distinguishing between partial discharges based on the UHF detection technique'. Int. Conf. Condition Monitoring and Diagnosis (CMD), Beijing, China, April 2008, pp. 1060–1064

10 Chang, C.S., Jin, J., Chang, C., Hoshino, T., Hanai, M., Kobayashi, N.: 'Separation of corona using wavelet packet transform and neural network for detection of partial discharge in gas-insulated substations', *IEEE Trans. Power Deliv.*, 2005, **20**, (2), Part: 2, pp. 1363–1369

11 Jin, J., Chang, C.S., Chang, C., Hoshino, T., Hanai, M., Kobayashi, N.: 'Classification of partial discharge events in gas insulated substations using wavelet packet transform and neural network approaches', *IEE Proc. Sci. Meas. Technol.*, 2006, **153**, (2), pp. 55–63

12 Yang, L., Judd, M.D., Bennoch, C.J.: 'Denoising UHF signal for PD detection in transformers based on wavelet technique'. Proc. Conf. Electrical Insulation and Dielectric Phenomena, Colorado, USA, October 2004, pp. 166–169

13 Florkowski, M., Florkowska, B.: 'Wavelet-based partial discharge image denoising', *IET Gener. Transm. Distrib.*, 2007, **1**, (2), pp. 340–347

14 Zhou, C., Hepburn, D.M., Song, X., Michel, M.: 'Application of denoising techniques to PD measurement utilising UHF, HFCT, acoustic sensors and IEC60270'. Int. Conf. Electricity Distribution – Part 1, Prague, Czech, June 2009, pp. 1–4

15 Aminghafari, M., Cheze, N., Poggi, J.M.: 'Multivariate de-noising using wavelets and principal component analysis', *Comput. Stat. Data Anal.*, 2006, **50**, pp. 2381–2398

16 Lopez-Roldan, J., Tang, T., Gaskin, M.: 'Optimisation of a sensor for onsite detection of partial discharges in power transformers by the UHF method', *IEEE Trans. Dielectr. Electr. Insul.*, 2008, **15**, (6), pp. 1634–1639

17 Kemp, I.J.: 'Partial discharges and their measurement', in Warne, D.F. (Ed.): 'Advance in high voltage engineering' (IEEE Press, 2004, 1st edn.), pp. 139–190

18 Agoris, P., Meijer, S., Smit, J.J.: 'Sensitivity check of an internal VHF/UHF sensor for transformer partial discharge measurements'. The Powertech'07 Conf., Lausanne, France, July 2007, pp. 2065–2069

19 Ando, A., Kagoshima, K., Kondo, A., Kubota, S.: 'Novel microstrip antenna with rotatable patch fed by coaxial line for personal handy-phone system units', *IEEE Trans. Antennas Propag.*, 2008, **56**, (8), pp. 2747–2751

20 Ju, T., Zhongrong, X., Xiaoxing, Z., Caixin, S.: 'GIS partial discharge quantitative measurements using UHF microstrip antenna sensors'. Conf. Electrical Insulation and Dielectric Phenomena (CEIDP), Vancouver, Canada, October 2007, pp. 116–119

21 Roy, A., Ghosh, S., Chakrabarty, A.: 'Wideband performance of dielectric loaded monopole trans-receive antenna system'. Int. Conf. Industrial and Information Systems (ICIIS), Colombo, Sri Lanka, August 2007, pp. 181–185

22 Sinaga, H.H., Phung, B.T., Blackburn, T.R.: 'Design of ultra high frequency sensors for detection of partial discharges'. Proc. Int. Symp. High Voltage Engineering, Cape Town, South Africa, October 2009, pp. 892–896

23 Chen, E., Chou, S.Y.: 'Characteristics of coplanar transmission lines on multilayer substrates: modeling and experiments', *IEEE Trans. Microw. Theory Tech.*, 1997, **45**, (6), pp. 939–945

24 Katsuse, T., Kirishima, T., Morita, A., Ohtsuka, S., Hikita, M.: 'Partial discharge characteristics in UHF-band of composite insulation system including various artificial defects in transformer'. Int. Conf. Condition Monitoring and Diagnosis (CMD), Beijing, China, April 2008, pp. 68–73

25 Raja, K., Devaux, F., Lelaidier, S.: 'Recognition of discharge sources using UHF PD signatures', *IEEE Electr. Insul. Mag.*, 2002, **18**, (5), pp. 8–14

26 Denissov, D., Köhler, W., Tenbohlen, S., Grund, R., Klein, T.: 'Wide and narrow band PD detection in plug-in cable connectors in the UHF range'. Int. Conf. Condition Monitoring and Diagnosis, Beijing, China, April 2008, pp. 1056–1059